










Towards Increasing Robot Autonomy in CHARM Facility: Network Performance, 3D Perception, and Human Robot Interface

David Forkel^{1,2}^a, Pejman Habibiroudkenar^{1,3}^b, Enric Cervera², Raúl Marín-Prades²^c,
Lucas Comte¹^d, Eloise Matheson¹^e, Christopher McCreavy¹^f, Luca Buonocore¹^g,
Josep Marín-Garcés¹^h and Mario Di Castro¹ⁱ

¹European Organization for Nuclear Research (CERN), Meyrin, Switzerland

²Jaume I University, Castellón de la Plana, Spain

³Aalto University, Espoo, Finland

{david.guenter.forkel, pejman.habibiroudkenar, lucas.philippe.comte, eloise.matheson, christopher.mcgreavy,
luca.rosario.buonocore, josep.marin.garces, mario.di.castro}@cern.ch,
{ecervera, rmarin}@uji.es

Keywords: Mobile Robotics, Wireless Communication, 3D Fusion, Human-Robot Interaction.

Abstract: The CHARMBot robot performs remote inspections in CERN's CHARM facility, with its operations currently managed through teleoperation. This study investigates the challenges and potential solutions to enhance CHARMBot's autonomy, focusing on network performance, 3D perception, and the graphical user interface (GUI). The communication network can experience constraints, as demonstrated in Experiment 1, which highlights the latency in transmitting compressed images to the operator at the control station. Under certain conditions, this latency can significantly impact manual control, leading to TCP buffer congestion and displaying images to the user with a delay of up to 10 seconds, depending on the network congestion, requested resolution and compression rate. To improve user interaction and environmental perception, CHARMBot needs to be equipped with advanced sensors such as 3D LiDAR and stereo camera. Enhancing the robot's autonomy is crucial for safe interventions, allowing the remote operator to interact with the robot via a supervised interface. The experiments characterize the network's performance in transmitting compressed images and propose a "lightweight" visualization mode. Preliminary experiments on 3D perception using LiDAR and stereo camera and mesh creation of the environment are discussed. Future work will focus on better integration of these components and conducting a proof-of-concept experiment to demonstrate the system's safety.

1 INTRODUCTION


This article first describes the operational environment of the experiments. Subsequently, the importance of robotics at CERN and the role of the CHARMBot are emphasized. The Human Robot Interface is then presented for operational use and for 3D perception. Thereafter, the experiments on net-


work performance as well as point cloud map generation and mesh creation are conducted. The article ends with the conclusions from the experiments and further work.


1.1 The CERN High-Energy Accelerator Mixed-Field (CHARM) Facility


CHARM facility is a unique irradiation infrastructure at CERN, long utilized for testing electronic equipment used in CERN accelerators and accessible to users from the aerospace industry (CERN, 2024b).


CHARM offers a novel, cost-effective approach to radiation qualification. It enables the parallel batch screening of multiple components or boards and the testing of large systems, ranging from full racks


^a <https://orcid.org/0000-0001-5678-6186>


^b <https://orcid.org/0000-0001-5678-6186>


^c <https://orcid.org/0000-0002-2340-4126>

^d <https://orcid.org/0009-0006-6876-2783>

^e <https://orcid.org/0000-0002-1294-2076>

^f <https://orcid.org/0000-0001-8424-1941>

^g <https://orcid.org/0000-0001-5396-2519>

^h <https://orcid.org/0000-0002-5400-3480>

ⁱ <https://orcid.org/0000-0002-2513-967X>

to medium-sized satellites, under operational conditions. A notable application was the testing of the CELESTA CubeSat's radiation model before its space-flight, marking the first system-level test of an entire satellite. The facility is highly adaptable, providing a high-penetration radiation environment with adjustable maximum dose rates and fluxes through various configurations of target, shielding, and location. Space applications particularly benefit from CHARM's capability to simultaneously test the three main radiation effects of interest: single event effects, total ionizing dose, and displacement damage. The radiation environment generated at CHARM is also ideal for atmospheric neutron characterization of avionic systems.

In 2018, CERN established a commercial agreement with Innovative Solutions In Space (ISIS) BV, a Dutch company specializing in nanosatellite solutions (CERN, 2024c). In September 2018, ISIS experts conducted tests at CERN on two CubeSat systems that had previously flown multiple times, allowing for direct comparisons between ground testing and flight data. Future plans include offering ISIS customers the opportunity to perform irradiation tests at CHARM. Additionally, a test campaign in November 2018 supported the development of a radiation-tolerant micro-camera for satellite applications, in collaboration with MicroCameras & Space Exploration SA.



Figure 1: Radiation testing of CELESTA satellite in CHARM facility (CERN, 2024a).

1.2 The Importance of Robotics at CERN

CERN has a long-standing tradition of using robots for inspection, especially when dealing with highly radioactive components like ISOLDE targets (Catherall et al., 2017). Among these innovations is the Train-Inspection-Monorail (TIM) robot, specifically designed for the LHC. TIM integrates an electrical

train with a monorail system originally built for the Large-Electron-Positron (LEP) Collider. This versatile robot is employed for a variety of tasks, including visual inspections, functional tests of the 3,600 beam-loss monitors, and conducting radiation surveys within the LHC accelerator tunnel (Castro et al., 2018). This not only helps to reduce accelerator downtime but also significantly decreases the need for human intervention in potentially hazardous environments. Additionally, the Measurement & Inspection Robot for Accelerators (MIRA) is utilized for performing auto-piloted robotic radiation surveys in the SPS, further exemplifying CERN's commitment to enhancing the identification of beam-losses and efficiency in radiological risk planning through robotic technology in the accelerator complex (Forkel et al., 2023). In the CHARM facility, a frame with the integrated test components is changed weekly. The installed frame is picked up with an automated guided vehicle (AGV) in the target zone and placed in the shielded stock area. The frame prepared with the new devices is then picked up by the AGV and placed back in the target area. As this test device frame has to be placed very precisely, it was necessary to install cameras to monitor the exact positioning. In addition, further frames containing test devices are conveyed into the target area via monorails on the ceiling and near the wall. However, the gamma radiation dose in the target area is high enough for unprotected cameras to fail after just a few weeks, starting with individual dead pixels and ending with the camera failing completely as a result. It was therefore necessary to develop a robust robotic solution that could perform the visual inspection in the CHARM target area. In recent years 3D LiDAR sensing devices have become more compact and affordable, so a small robot platform can easily incorporate one such sensor together with a compact stereo vision system. The main advantage of combining 3D LiDAR with stereo cameras is the robustness against different conditions of the environment (Nickels et al., 2003). Also, dense stereo data fills the gaps in the sparse 3D LiDAR cloud (Maddern and Newman, 2016). The combination of both sensors can improve object tracking (Dieterle et al., 2017) and long-range depth estimation (Choe et al., 2021).

1.3 CHARMBot - Mobile Robot Base for Remote Inspection of Target Exchange

CERN has developed a new robot base for remote inspection of the target exchange at CHARM facility, the so-called CHARMBot. It follows the CERN-

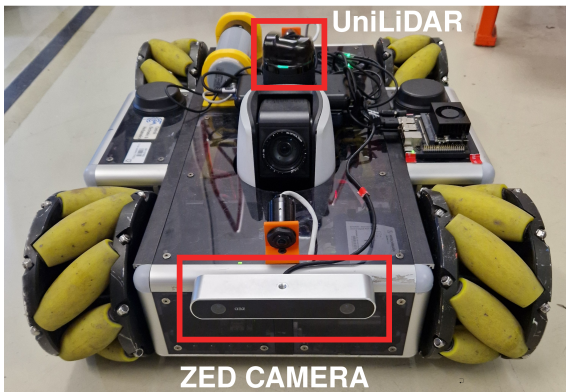


Figure 2: CHARMBot equipped with 3D LiDAR and stereo camera.

Bot modular robotic system, which consists of a mobile Mecanum wheel base, as well as the necessary sensors such as gamma radiation sensor and front and back cameras (Di Castro et al., 2018). Furthermore, the mechanical design features a robust and rigid structure made from aluminum profiles, which not only enhances durability but also ensures the protection of internal components. Since the main task lies in remote inspection, CHARMBot is equipped with a 360° surveillance camera located at the center of the robot. For the experiments described in this article, a 3D LiDAR with integrated IMU and a stereo camera were mounted on the robot base. In order to process the data, they were linked to a Nvidia Jetson Orin nano. One of the key features of CHARMbot is its compact size. The robot is specifically designed to fit beneath the target transporting racks, enabling it to access all areas of the CHARM facility. This ensures that no part of the inspection zone is overlooked. Overall, CHARMbot's innovative features and user-centric design make it an invaluable tool for visual inspection operations, offering a unique combination of precision, flexibility, and ease of use.

CHARMbot is primarily employed for visual inspection operations, with its main objective being to provide a comprehensive perspective of the CHARM target in areas where cameras are not installed. This capability allows for a thorough visual inspection of the entire area from a moving robot platform.

To achieve this, multiple advanced features have been integrated into Charmbot. The design philosophy was to create a plug-and-play solution, ensuring ease of use for operators. Consequently, several *systemd* services were developed that automatically initiate all communication points as soon as the robot is powered on.

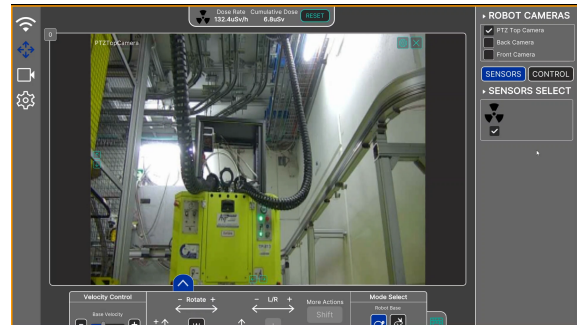


Figure 3: 2D GUI in operation during CHARM target exchange.

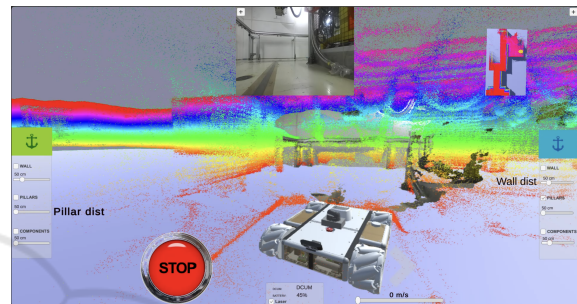


Figure 4: 3D Perception and Autonomous Navigation GUI overlaying the 3D LiDAR scan, visual odometry localization, and current point cloud from stereo camera.

1.4 Human Robot Interface for Teleoperation and Visual Inspection

Moreover, a sophisticated solution for managing the video streams from all onboard cameras has been implemented. This includes the ability to control the volume of data requested from each camera, optimizing the robot's performance under various conditions. Currently, two parameters can be adjusted: the video quality and the number of frames per second (FPS). By fine-tuning these settings, operators can maintain control of the robot even when bandwidth is limited, by reducing the video quality to the minimum necessary level. This adaptability enhances the overall efficiency and effectiveness of the inspection process. Besides this, as can be shown in Experiment 1, for highly congested network situations a camera visualization lightweight mode has been tested, to reduce the number of packets in transit while monitoring the cameras.

The control application for Charmbot is developed using the Unity game engine and features a 2D user interface. This interface is designed to be safe, intuitive, and user-friendly, ensuring that operators can manage the robot with ease. The GUI provides users with the flexibility to choose their preferred control device, enhancing accessibility and convenience

(Szczurek et al., 2023). Also, the operational tele-operated GUI is being upgraded to a supervised one, which enables activating high level navigation commands and representing 3D Mixed Reality information (see Figure 4). Moreover, the GUI provides an augmented reality mode, enabling the operator to inspect the remote intervention in a 3D hologram, which can be moved and scaled according to the user needs, so that the mission monitoring is more immersive for the operator (see Figures 5 and 6).

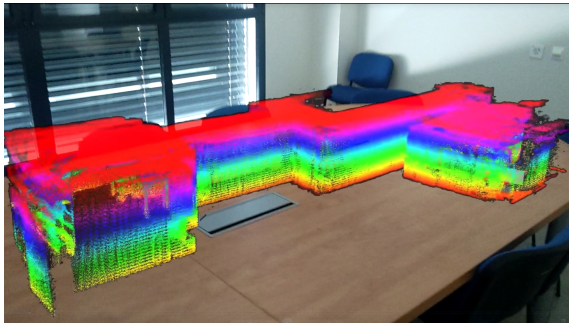


Figure 5: Augmented Reality GUI mode showing the exterior view of the CHARM facility.

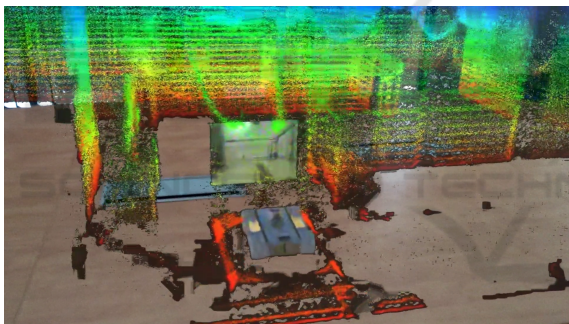


Figure 6: Augmented Reality GUI mode showing the map scaled and focusing on the robot position.

2 EXPERIMENTS

2.1 Experiment 1: Network Performance

In this experiment, a connection to CHARMbot is established from the ground station, where the human operator is located. It was observed that the cameras on CHARMBot, which use the Motion JPEG (MJPEG) protocol, experienced fluctuating frame retrieval times depending on the network state. As the Transmission Control Protocol (TCP) buffers began to fill, the overall delay increased by several seconds, which was not comfortable for the operator. The cam-

eras transmit images at a constant bit rate, according to the GUI parameters, via the MJPEG protocol.

To mitigate this issue, a network performance experiment was conducted, testing the Frame Retrieval Time (FRVT) under different configurations (i.e., compressions, resolutions). Results indicated that using a light-weight mode for camera visualization, employing single JPEG REST requests, can significantly improve performance under congestion situations. In this mode, the camera MJPEG connection is closed, and image feedback is provided through successive web JPEG requests. This allows the operator to select this mode if network performance degrades, ensuring that only one image is in transit at any given time, thereby preventing TCP buffer overload.

Figure 7 illustrates the JPEG compression size at different resolutions, highlighting the average frame size for each combination using CHARMBot’s WiFi connection and VPN encrypted tunneling. This helps to understand the data load each image imposes on the network. Moreover, Figure 8 demonstrates the Frame Retrieval and Visualization Time, which involves sending a packet to the robot to obtain a new image and waiting for it to be received and visualized before requesting the next one. This figure provides insights into the time taken for each frame retrieval and visualization cycle under various network conditions. Lastly, Figure 9 summarizes the Frames Per Second (FPS) that can be achieved in the light-weight mode at different resolutions when only a single image is in transit within the network, avoiding buffer overload. This mode results in FPS ranging from 2 to 10. These findings support the proposed light-weight mode for camera visualization in the GUI, enhancing operator experience by reducing delays and preventing TCP buffer overload under constrained network conditions.

2.2 Experiment 2: 3D LiDAR and Stereo Camera Map and Mesh Creation

2.2.1 Cloud Map Creation

In this experiment, CHARMbot is operated through teleoperation, navigating from the charging station located in the stocking area to the target area.

During the operation, point cloud data was collected from both the Unitree LiDAR and Zed stereo camera systems, along with integrated IMU values from the Unitree LiDAR and visual odometry provided by the stereo Zed camera. The Point-LIO (He et al., 2023) and RTABmap (Labbé and Michaud,

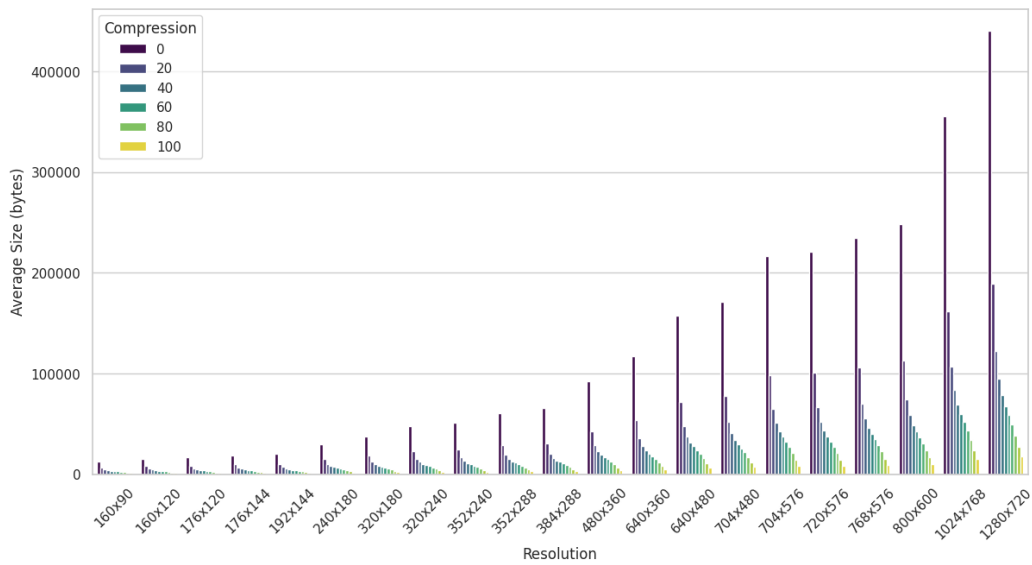


Figure 7: JPEG Compression Average Frame Size (100 images per combination) from CHARMBot using the WiFi connection and VPN encrypted tunneling , for every compression and resolution.

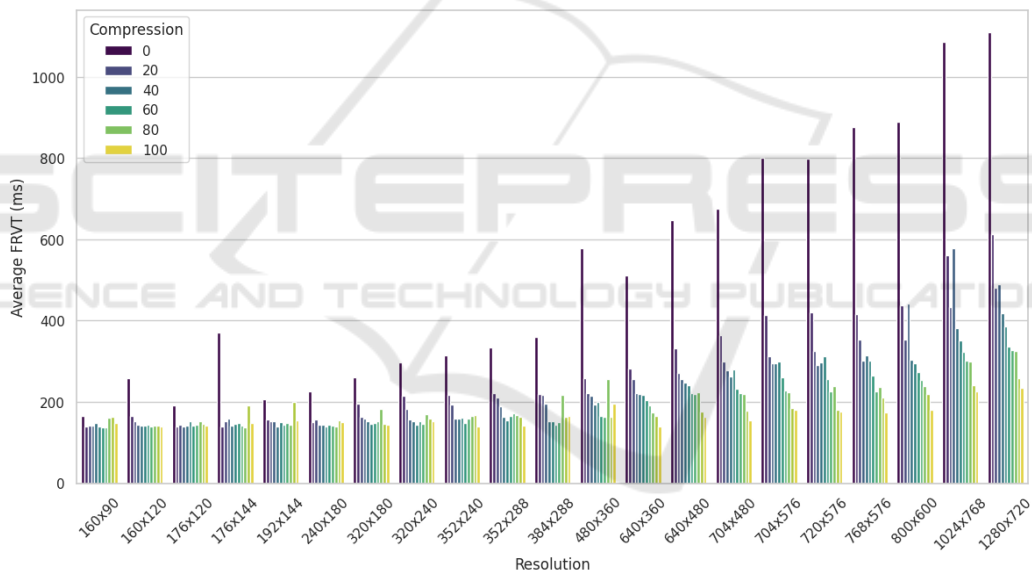


Figure 8: Frame Retrieval and Visualization Time (FRVT) to the ground station from CHARM facilities using the WiFi connection and VPN encrypted tunneling.

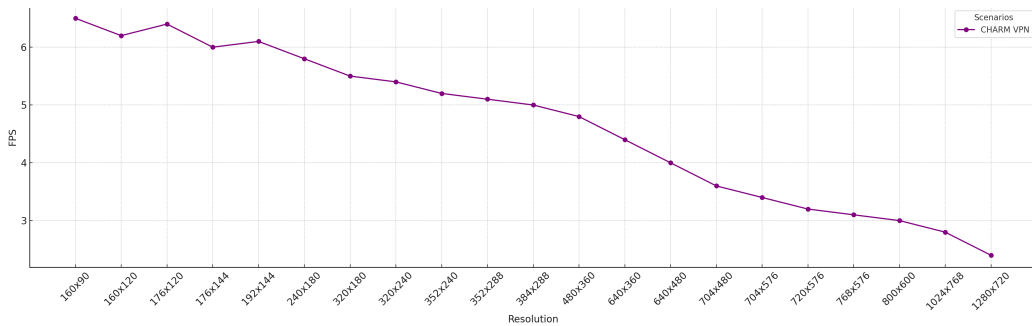


Figure 9: Summary of REST Lightweight mode Frame Per Seconds using WiFi connection and VPN encrypted tunneling.

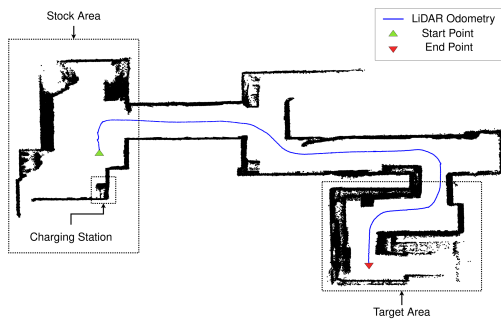


Figure 10: Schematics of the CHARM facility and CHARMbot's LiDAR localization.

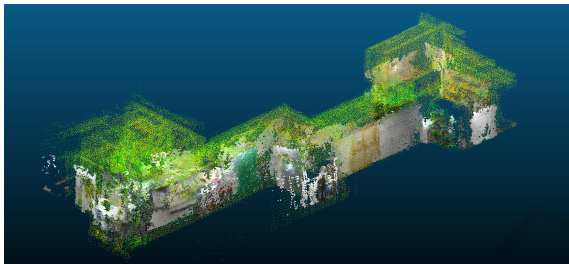


Figure 11: CHARM facility cloud map created using Uni-tree LiDAR and Zed stereo camera points.

2018) algorithms were employed to generate cloud maps from the LiDAR and Zed stereo camera data, respectively. Minor modifications were made, wherein LiDAR scan matching and IMU fusion odometry were utilized as inputs for RTABmap algorithm. The schematics of CHARM facility and the LiDAR odometry are shown in Figure 10. Upon creating the point cloud, points above the ceiling and below the floor that were falsely registered by RTABmap were removed. Furthermore, due to dynamic points present at the site, excessive noise was registered in RTABmap's cloud. This problem was mitigated by first constructing an octree for both the LiDAR and camera point clouds, then finely aligning the point clouds using Iterative Closest Point (ICP) and eliminating points from the RTABmap output that exceeded the tolerance distance threshold. The filtered cloud was a dense, well-aligned, and information-rich point cloud depicted in Figure 11. The processed cloud map was utilized in the GUI to visualize the real-time position of the robot.

2.2.2 Meshing

Once the map is created, statistical outlier removal was used to eliminate sparse points. This step ensures that the points adversely affecting the meshing accuracy are removed. The point cloud is then sub-sampled to reduce the computational power required for further processing. Next, each point's nor-

malis are calculated using the triangulation method to indicate the direction each point is facing, which is essential for accurately reconstructing the surface of the object. With the knowledge of normals at hand, the Poisson surface reconstruction function in CloudCompare (CloudCompare, 2023) is used to create the mesh. This method converts the point cloud data into a continuous surface, resulting in a detailed mesh that accurately represents the scanned object. The Poisson method is particularly effective at handling complex shapes, making it ideal for creating high-quality meshes. The process can inevitably produce incorrect meshes. To alleviate this challenge, a density scalar field is utilized to remove inaccurate meshes by taking the 99% dense meshes and removing the rest, as shown in Figure 13, ensuring the final model is as precise as possible. The meshing process is summarized in Figure 12.

2.3 Video

Under the following link the video of the GUI supervising the robot inspection is shown. The 3D Mixed Reality, visual-odometry localization, and pre-registered 3D LIDAR overlay are demonstrated here: <https://cernbox.cern.ch/s/gcjF5wtMmgSZLVX>

3 CONCLUSIONS AND FURTHER WORK

This paper addresses the current challenges and proposes solutions to enhance CHARMBot's autonomy through the optimization of the communication network, 3D perception, and GUI, as well as the integration of AI. In fact, enhancing the autonomy of CHARMBot within the CHARM facility is critical, particularly under constrained network environments. Autonomous capabilities allow CHARMBot to operate more effectively and safely, even when network performance is degraded. By equipping CHARMBot with advanced sensors such as 3D LiDAR and stereo cameras, we can ensure robust environmental perception and efficient task execution. This reduces the reliance on constant manual teleoperation, which can be significantly hampered by network latency and bandwidth limitations. The experiments conducted have demonstrated that employing a lightweight visualization mode can mitigate TCP buffer congestion and improve the operator's experience, maintaining control over the robot even in challenging network conditions. Additionally, designing a supervised user interface is paramount for the safe operation of CHARMBot in hazardous scenarios like those

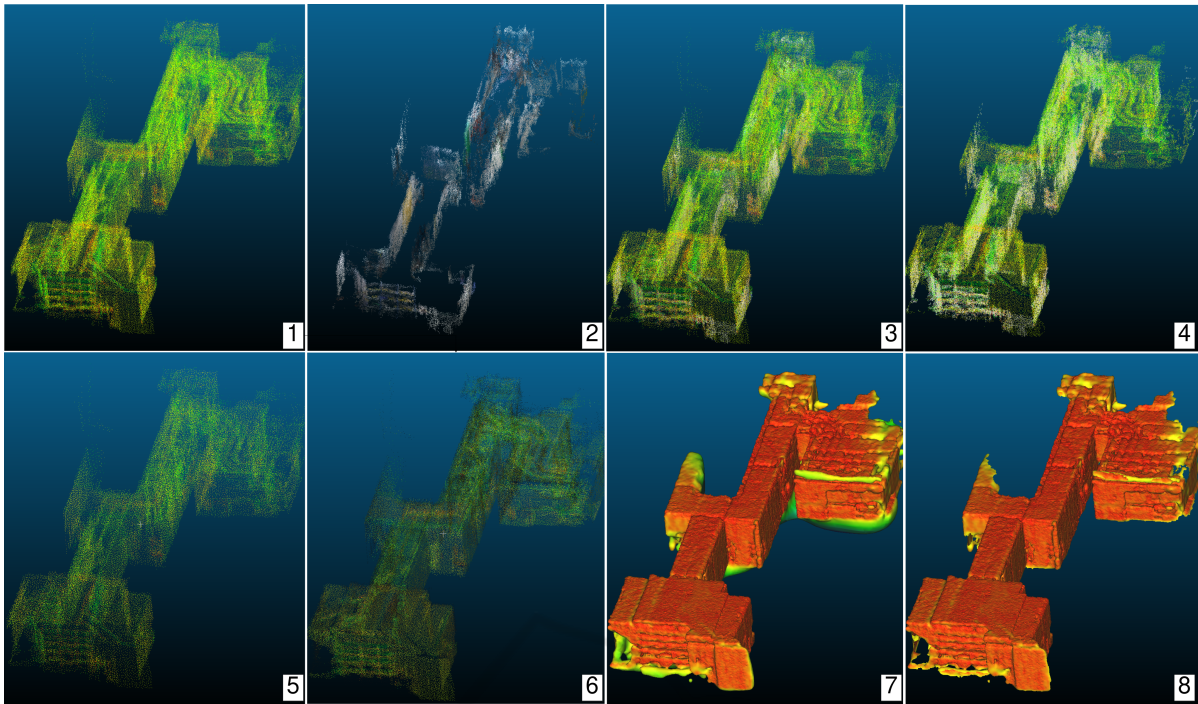


Figure 12: Process of creating a mesh from a LiDAR point cloud, The map created using LiDAR [1] and the map created from a stereo camera [2] are merged [3] and processed through several steps: statistical outlier removal [4] for noise reduction, sub-sampling [5] for data simplification, normal calculation using the triangulation method [6], and ultimately mesh creation [7]. The final step involves using a density scalar field to remove inaccurate meshes, ensuring the precision of the model [8].

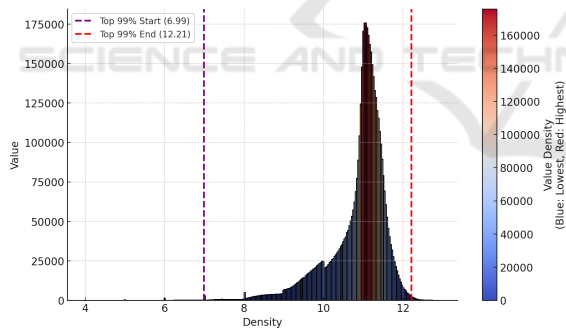


Figure 13: The scalar field highlights the top 99% dense areas to ensure the accuracy and quality of the mesh by filtering out less significant regions.

present in the CHARM facility. By integrating these autonomous behaviour and user interface enhancements, CHARMBot can perform critical inspections and tasks with higher reliability and reduced human risk, aligning with CERN’s commitment to leveraging advanced robotics for safer and more efficient operations. Future work will focus on the further integration of these components and conducting proof-of-concept experiments to demonstrate the proposed system’s safety.

AUTHORS’ CONTRIBUTIONS

The authors confirm contribution to the article as follows. Implementation and experimentation David Forkel, Pejman Habibiroudkenar, Enric Cervera, Raúl Marín-Prades, Lucas Comte and Josep Marin-Garcés; Concept and supervision Eloise Matheson, Christopher McGreavy, Lucas Buonocore and Mario Di Castro.

ACKNOWLEDGEMENTS

This work has been funded by CERN (European Organization for Nuclear Research). Special thanks to Mr. Jérôme Lendaro for his technical support in experimental phases.

REFERENCES

- Castro, M. D., Tambutti, M. L. B., Ferre, M., Losito, R., Lunghi, G., and Masi, A. (2018). i-tim: A robotic system for safety, measurements, inspection and maintenance in harsh environments. In *2018 IEEE International Symposium on Safety, Security, and Rescue*

- Robotics, SSRR 2018, Philadelphia, PA, USA, August 6-8, 2018*, pages 1–6. IEEE.
- Catherall, R., Andreatza, W., Breitenfeldt, M., Dorsival, A., Focker, G., Gharsa, T., Giles, T., Grenard, J.-L., Locci, F., Martins, P., Marzari, S., Schipper, J., Shornikov, A., and Stora, T. (2017). The isolde facility. *Journal of Physics G: Nuclear and Particle Physics*, 44.
- CERN (2024a). Cern aerospace facilities, url: <https://kt.cern/aerospace/facilities> (accessed 20.07.2024).
- CERN (2024b). Charm - mixed fields, url: <https://kt.cern/technologies/charm-mixed-fields> (accessed 20.07.2024).
- CERN (2024c). First commercial customers in charm, url: <https://kt.cern/success-stories/first-commercial-customers-charm> (accessed 20.07.2024).
- Choe, J., Joo, K., Imtiaz, T., and Kweon, I. S. (2021). Volumetric propagation network: Stereo-lidar fusion for long-range depth estimation. *IEEE Robotics and Automation Letters*, 6(3):4672–4679.
- CloudCompare (2023). Cloudcompare 3d point cloud and mesh processing software. Version 2.11.3.
- Di Castro, M., Ferre, M., and Masi, A. (2018). Cern-tauro: A modular architecture for robotic inspection and telemanipulation in harsh and semi-structured environments. *IEEE Access*, 6:37506–37522.
- Dieterle, T., Particke, F., Patino-Studencki, L., and Thielecke, J. (2017). Sensor data fusion of lidar with stereo rgb-d camera for object tracking. In *2017 IEEE Sensors*, pages 1–3. IEEE.
- Forkel, D., Cervera, E., Marín, R., Matheson, E., and Di Castro, M. (2023). Mobile robots for teleoperated radiation protection tasks in the super proton synchrotron. In Gini, G., Nijmeijer, H., Burgard, W., and Filev, D., editors, *Informatics in Control, Automation and Robotics*, pages 65–82, Cham. Springer International Publishing.
- He, D., Xu, W., Chen, N., Kong, F., Yuan, C., and Zhang, F. (2023). Point-lio: Robust high-bandwidth light detection and ranging inertial odometry. *Advanced Intelligent Systems*, 5.
- Labbé, M. and Michaud, F. (2018). Rtab-map as an open-source lidar and visual simultaneous localization and mapping library for large-scale and long-term online operation. *Journal of Field Robotics*, 36.
- Madden, W. and Newman, P. (2016). Real-time probabilistic fusion of sparse 3d lidar and dense stereo. In *2016 IEEE/RSJ International Conference on Intelligent Robots and Systems (IROS)*, pages 2181–2188. IEEE.
- Nickels, K., Castano, A., and Cianci, C. (2003). Fusion of lidar and stereo range for mobile robots. In *Int. Conf. on Advanced Robotics*.
- Szczurek, K. A., Prades, R. M., Matheson, E., Rodriguez-Nogueira, J., and Castro, M. D. (2023). Multimodal multi-user mixed reality human-robot interface for remote operations in hazardous environments. *IEEE Access*, 11:17305–17333.